A new determination method of interatomic potential for sodium silicate glass simulations

A New Determination Method of Interatomic Potential for Sodium Silicate Glass Simulations

Yuya Yamamoto[a*], Naoya Sawaguchi[a] and Makoto Sasaki[a]

[a]Muroran Institute of Technology, 27-1, Mizumoto-cho, Muroran, Hokkaido 050-8585, Japan

Corresponding author: Yuya Yamamoto

Muroran Institute of Technology
27-1, Mizumoto-cho, Muroran, Hokkaido 050-8585, Japan

Phone: +81-143-46-5673

E-mail: 16096004@mmm.muroran-it.ac.jp

Abstract

An interatomic potential for the classical molecular dynamics (MD) simulation of sodium silicate glasses was proposed. The ionic charges for this interatomic potential were determined by Mulliken population analysis via the density functional theory (DFT) calculation of alkali silicate crystals. The Si-O interatomic potential energy curve was determined by molecular orbital (MO) calculation of SiO^{2+}. The results of classical MD simulations using the new interatomic potential were consistent with the experimental trends in interatomic distance, thermal expansion coefficient, molar volume, Si-O-Si bond angle distribution, and Q_n ratio with respect to the sodium composition of the silicate glass. The proposed interatomic potential improves the reproducibility of the ring size distribution in silicate glasses compared to conventional potentials.

Key words: molecular dynamics simulation, sodium silicate glasses, first-principles calculation, material design

1. Introduction

The physical properties of glasses, including the self-diffusion coefficient of ions, electrical conductivity, thermal expansion, bulk modulus, specific heat, and glass transition temperature, are known to be related to the glass composition. For example, the thermal expansion coefficient of sodium silicate glasses increases with increasing Na_2O/SiO_2 ratio [1]. This effect is attributed to the change in atomic structure from a three-dimensional network structure to a two-dimensional flexible structure as the Na_2O/SiO_2 ratio increases [2]. Because the physical properties of glasses are closely related to the atomic structures of those glasses, the

development of techniques to predict glass properties based on glass composition is important for the study of new functional glasses.

First-principles calculations have been widely used to investigate new functional crystals. However, simulations of glasses involve many nuclei and electrons, and the nonperiodic structures of glasses require large calculation models. In addition, the derivations of the self-diffusion and viscosity coefficients of glasses require calculations with long time scales [3]. Molecular dynamics (MD) simulations based on classical mechanics are suitable for the investigation of glasses because of their lower computational cost compared to first-principles calculations.

Interatomic potential function for application in classical MD simulations of oxide glasses have been developed using first-principles calculations. The interatomic potentials for Si-O, P-O, and Al-O pairs were determined from first-principles calculations of tetrahedron clusters [4-7]. These interatomic potentials were then applied to classical MD simulations of silicate crystals/glasses, aluminophosphate crystals, and aluminosilicate crystals [4-7]. The development of these interatomic potentials has enhanced the reliability of classical MD simulations; however, this method, used to derive the above potentials, cannot necessarily be applied to generate the interatomic potentials needed to simulate all oxide glasses.

Silicate, aluminosilicate, and phosphate glasses essentially form only tetrahedral structural units, whereas borate glasses are formed by two structural units: BO_3 and BO_4. In these cases, the interatomic potentials cannot be easily derived from first-principles cluster calculations. Cluster models for the first-principles calculation of glasses without experimental structural data are also difficult to obtain.

The Si-O bonds in SiO_2 glass are weakened when network-modifying oxides (e.g., Li_2O and Na_2O) are introduced [8]. Noritake et al. [9] and Cormack et al. [10] used empirical formulae to determine the charges of silicon and oxide ions as functions of the Na_2O/SiO_2 ratio in sodium silicate melts/glasses for classical MD simulation. Sawaguchi et al. [11] also simulated lithium borate glasses/melts using classical MD with ionic charges determined by empirical equations depending on the Li_2O/B_2O_3 ratio. However, no method to determine the optimal ionic charges based on glass composition for use in classical MD simulation has been established.

The target of this study is sodium silicate glass, which is a basic component of practical glasses. First, choosing a function as the interatomic potentials applying to classical MD simulations of the glasses, then we studied a method of finding an appropriate parameter values appeared in the potential function by first-principles calculations. The Si-O bond distance does not vary with glass composition [12-15], suggesting that the equilibrium distance of the Si-O interatomic potential must be fixed independent of the glass composition at ordinary temperature and pressure. In contrast, the charges of silicon and oxide ions are thought to depend on glass composition; this dependency is considered to contribute to the weakening of the Si-O bond with increasing alkali oxide ratio in silicate glasses [8]. This relationship must be reflected in the depth of the Si-O interatomic potential for each glass composition.

In this study, an Si-O interatomic potential was developed based on the results of nonempirical molecular orbital (MO) calculations of an SiO^{2+} cluster. We selected this diatomic molecular cluster so that the coordination number of the polyhedron can correspond with changes due to temperature and pressure [16].

Based on these calculations, the shape of the Si-O interatomic potential function was fixed, with the exception of the potential depth, which changed with glass composition. The ion charges of silicate glasses were estimated from the results of density functional theory (DFT) calculations of alkali silicate crystals with related sodium silicate glass composition. The results of the two different calculations were combined to develop the complete Si-O interatomic potential function. Finally, a unique interatomic potential for the classical MD simulation of sodium silicate glass was obtained for each glass composition as described by the Na_2O/SiO_2 ratio. MD simulations of sodium silicate glasses with several compositions were then performed using the obtained interatomic potentials, and the results were evaluated using experimental results.

2. Determination Method of Interatomic Potentials

2-1. Interatomic Potential Function

In this study, we applied the interatomic potential function reported by Sakuma et al. [17], which has been shown to accurately reproduce the physical properties and structures of oxide crystals. The interatomic potential, $U_{ij}(r_{ij})$, is shown in

$$U_{ij}(r_{ij}) = \frac{z_i z_j e^2}{4\pi\varepsilon_0 r_{ij}} + f_0(b_i + b_j)\exp\left(\frac{a_i + a_j - r_{ij}}{b_i + b_j}\right) - \frac{c_i c_j}{r_{ij}^6} + \left\{D_{1ij}\exp(-\beta_{1ij} r_{ij}) - D_{2ij}\exp(-\beta_{2ij} r_{ij})\right\} \quad (1)$$

where r_{ij} is the distance between ions i and j. The first term is the Coulomb force term, where z is the ionic charge, ε_0 is the dielectric constant of vacuum, and e is the elementary charge. The second term is the short repulsive force term, where a_i and b_i are parameters, and the third term is the van der Waals force term with

parameter c_i. The fourth term is added as a covalent force term to account for Si-O interactions, where D_{1ij}, β_{1ij}, D_{2ij}, and β_{2ij} are parameters. The constant f_0 is 4.185 kJ nm^{-1} mol^{-1}.

2-2. Determination of Ionic Charges

The ionic charges z_i were determined by DFT calculations of alkali silicate crystals using the CASTEP code [18]. A plane-wave basis and norm-conserving pseudopotential method with the GGA PBE exchange-correlation function [19] were applied. The target crystals [20-32] and applied *k*-point set are listed in Table 1. The charges of ions in crystals of lithium silicate and potassium silicate systems were also calculated for comparison. The following norm-conserving pseudopotentials were used: Li, $2s^1$; Na, $2s^22p^63s^1$; K, $3s^23p^64s^1$; Si, $3s^23p^2$; and O, $2s^22p^4$.

The crystal structures were optimized using a cutoff energy of 1500 eV and an SCF tolerance of 5.0×10^{-7} eV/atom. The optimized lattice parameters are listed in Table 1 along with error based on the literature values [20-32]. The largest error was 2.88%. The ionic charges z_i in (1) for silicate crystals were calculated from Mulliken population analysis [33, 34] for each crystal. The validity of this calculation method was confirmed by MD simulations of alkali silicate crystals and glasses in previous works [16, 35]. The cutoff distance used to count electrons belonging to each nucleus was fixed to 0.3 nm for all target crystals. Figure 1 shows the Mulliken charges of ions in alkali (*A*) silicate crystals with compositions of xA_2O-(1-x)SiO_2. The charges of the silicon and alkali ions decrease with increasing *x*. The absolute values of Mulliken charges are recognized as having low reliability [33]. MD simulations of sodium silicate glasses using charges based on the Hirshfeld

method [36], which is another charge analysis method, poorly reproduced the glass structures [16]. In contrast, the trends in Mulliken charge with chemical composition seem to be meaningful; thus, Mulliken charges were used in this study. The ionic charges z_{Na}, z_{Si}, and z_O were given by (2-1), (2-2), and (2-3), respectively, as functions of composition x:

$$z_{Na} = -0.25x + 1.0 \qquad (0 < x \le 1) \qquad (2\text{-}1)$$

$$z_{Si} = -0.50x + 2.4 \qquad (0 \le x < 1) \qquad (2\text{-}2)$$

$$z_O = -\frac{2x \cdot z_{Na} + (1-x) \cdot z_{Si}}{2-x} \qquad (0 \le x \le 1) \qquad (2\text{-}3)$$

The constants in (2-1) and (2-2) were determined in consideration of the empirical values of z_{Na} and z_{Si} used in a previous study [11]. Equation (2-3) for z_O was obtained from the charge neutrality of the crystals.

2-3. Determination of Parameters a_i, b_i, c_i, D_{1ij}, β_{1ij}, D_{2ij}, and β_{2ij} in the Interatomic Potential Function

The values of a_i, b_i, c_i, D_{1ij}, β_{1ij}, D_{2ij}, and β_{2ij} in (1) for the Si-O interatomic potential were determined by fitting an interatomic potential curve to an Si-O energy surface derived from a nonempirical MO calculation of an SiO^{2+} cluster model, as in [4, 5, 7]. The MO calculation used the Gaussian09 code [37] with the second-order Møller-Plesset (MP2) method [38] and 6-311+g(d) [39] basis set. The values of parameters a_i, b_i, c_i, D_{1ij}, β_{1ij}, D_{2ij}, and β_{2ij} for Si and O were determined for each x because the ionic charge z_i also depends on x, as shown in (2-1), (2-2), and (2-3). The reliability of the interatomic potential was confirmed by the reproducibility of the Si-O distance in the MD simulations of alkali silicate crystals.

Figure 2 shows the calculated Si-O potential energy surface and the fitting result for silicate glass (x = 0). The equilibrium Si-O distance derived from the SiO^{2+} model was 0.146 nm. Table 2 shows the determined interatomic potential parameters for each composition, where a_{Na}, b_{Na}, and c_{Na} are empirically determined values [9].

3. Classical MD Simulation Method

MD simulations of sodium silicate glasses were performed using the MXDORTO code [40] with a step time of 2.0 fs. The Ewald method was applied to calculate the Coulomb force and potential. Although constant-volume conditions were applied in previous works [10, 41, 42], the *NPT* ensemble was chosen in this work to allow the simulation of a wide temperature range. For each composition, 4950 particles (N) were placed in a cubic MD cell with side lengths of 4.5 nm using a random-number method. Next, 250,000 steps were run at 0.1 MPa (P) at 3000 K (T) for structural relaxation. It was confirmed that the internal energy became stable. The glassy state of the system was obtained using a stepwise cooling scheme with a cooling rate of 0.01 K/step. To obtain a stable state, isothermal simulation was performed following the cooling step using the following sequence: 250,000 steps at 3000–2100 K and 500,000 steps at 1800–300 K. The steps at 1800-300 K were increased step time for structural relaxation because the movement of ions in the process from melt to glass slows down. In order to investigate the glass structure at room temperature and the reproducibility of the expansion rate, 10,000 step analysis data of 300 K and 600K was used.

In this work, two different interatomic potentials were applied in MD simulations of glasses with different

compositions: (1) the interatomic potential derived in this work based on first-principles calculations, named IP1, and (2) the interatomic potential determined empirically in a previous work [11], named IP2. The abbreviations IP1 and IP2 are also used to denote the results of MD simulations using the respective potentials.

4. Results

Table 3 shows the MD simulation results for the first neighboring interatomic distances ($d_{Si\text{-}O}$ and $d_{Na\text{-}O}$) in sodium silicate glasses. The values of $d_{Si\text{-}O}$ and $d_{Na\text{-}O}$ were determined as the peak top position of the nearest peak of pair correlation function. The $d_{Si\text{-}O}$ values determined from IP1 simulations of glasses with different compositions are consistent with reported results based on X-ray diffraction [12], EXAFS [13-15], and crystal structure data [20-32]. Similarly, the values of $d_{Na\text{-}O}$ for all x determined by the IP1 simulations are consistent with EXAFS results [13-15] and crystal structure data [27, 28]. The values of $d_{Si\text{-}O}$ and $d_{Na\text{-}O}$ determined from the IP2 simulations are shorter than the IP1 values for all x.

Figure 3 shows the simulated molar volumes, V, of $x$$Na_2O$-(1-$x$)$SiO_2$ glasses. The IP1 simulations reproduced the downward trend in molar volume with increasing x reported in the literature [43, 44]; however, the absolute values of the IP1 molar volumes are larger than the literature values [43, 44]. The molar volumes of the IP2 simulations are consistent with the literature value [43, 44] for all x.

The thermal expansion coefficients of $x$$Na_2O$-(1-$x$)$SiO_2$ glasses were calculated by (3) using the molar volumes at 300 and 600 K:

$$\beta = \frac{1}{V_{300K}}\left(\frac{dV}{dT}\right) \qquad (3)$$

where V, T, and V_{300K} are the molar volume, temperature, and molar volume at 300 K, respectively. Figure 4 shows thermal expansion coefficients of xNa$_2$O-(1-x)SiO$_2$ glasses determined by MD simulations. The IP1 and IP2 simulations successfully reproduced the increasing trend in thermal expansion coefficient with increasing x along with the absolute values reported in the literature [2].

Figure 5 shows the distributions of O-Si-O bond angles ($\theta_{O\text{-}Si\text{-}O}$) and Si-O-Si bond angles ($\theta_{Si\text{-}O\text{-}Si}$) in the simulated xNa$_2$O-(1-x)SiO$_2$ glasses. The $\theta_{O\text{-}Si\text{-}O}$ distributions for the IP1 and IP2 simulations are centered at 109° for all x, and the distributions become sharper with increasing x. This suggests that strain on the SiO$_4$ tetrahedra in the glasses decreases with increasing x. The $\theta_{Si\text{-}O\text{-}Si}$ angles for the IP1 simulation are distributed between 120° and 180° for all x, whereas those for the IP2 simulation are distributed between 110° and 180°. The $\theta_{Si\text{-}O\text{-}Si}$ distribution of the IP1 simulation showed two peaks at 140° and 160° for x = 0. The distribution around 140° increased with increasing x. The distribution around 160° peak decreased with increasing x.

Q_n is the ratio of classified SiO$_4$ tetrahedron for all SiO$_4$ unit, where n indicates the number of bridging oxygen atoms in a unit [45]. Figure 6 shows the Q_n distribution of xNa$_2$O-(1-x)SiO$_2$ glasses at 300 K. In both the IP1 and IP2 simulations for x = 0 and 0.1, one or two three-coordinated silicon atoms were observed; these are recognized as abnormal structures caused by the limited simulation time scale and space. Therefore, the Q_n values were determined in exclusion of the three-coordinated silicon atoms. Maekawa et al. [46] investigated the variation in Q_n with x using ^{29}Si MAS-NMR for glasses with $0.2 \leqq x \leqq 0.4$ and reported that Q_2 and Q_3 increased with increasing x, whereas Q_4 decreased. The IP1 simulation better reproduced Q_n

compared to the IP2 simulation for $0.4 \leqq x \leqq 0.5$.

5. Discussion

Figure 7 shows the Si-O and Na-O Coulomb force $z_i z_j$ of IP1 and IP2 simulations. The Si-O of Coulomb force $z_{Si}z_O$ of IP1 and IP2 was increased with increasing x. Moreover, the IP1 simulations gradually increased in $z_{Si}z_O$ than the IP2 simulations. As shown in Table 2 (b), the $z_{Na}z_O$ of the IP2 simulations set by fixing the formal charge for all x. On the other hand, the charge of sodium of the IP1 simulations set so that it decreased as the x increased from the (2-1). The Na-O of Coulomb force $z_{Na}z_O$ of the IP1 simulations increases and the IP2 simulations decreases with increasing x. As denoted in Table 3, the Si-O bond lengths, $d_{Si\text{-}O}$, of glasses were greater in the IP1 simulation than in the IP2 simulation. This is attributed to the decrease in the Coulomb interaction between Si and O. The Na-O distances, $d_{Na\text{-}O}$, were also the same reason.

In generally, the interatomic potential for MD simulations of glasses is determined to reproduce the glass structures and the physical properties by trial and error [10, 11]. In the case of the conventional MD simulation of glasses [10, 11], the interatomic potential has been applied to even if the quantitative ratios of the elements were changed, as long as they were composed only of the same element. However, it had been found that applying the same interatomic potential to each composition deteriorates the reproducibility of the glass structure. For this reason, only the ionic charge (z_{Si} and z_O) of the Coulomb force term had been empirically responsible for the compositional change correspondence [11]. IP2 is also reproduced the molar volumes of literature value in sodium silicate glasses by trial and error. As shown in Figure 3, the molar volumes

determined by the IP2 simulations are consistent with literature values [43, 44]. However, the Si-O distances for every glass composition simulated by IP2 are shorter than corresponding literature values (Table 3), indicating that the glass structures simulated by IP2 are distorted. On the other hand, IP1 is determined for each composition by the first-principles calculations. Since the IP1 is not determined by trial and error, the time required for the setting procedure can be shortened over IP2. Figure 3 shows that the molar volumes of the IP1 simulation do not coincide with the literature [43, 44], although the decreasing tendency of molar volume as x increases from 0 to 0.5 is reproduced; we regard this tendency as important to understand the dependence of the glass structure on composition. The reproducibility of the value of physical properties and structure of glasses is deviated from the difference between the simulation and the actual system due to difference in environmental conditions. It is considered that the value of molar volume of IP1 simulation is larger than the literature value due to the influence of the fast cooling rate of simulation. In order to reduce the difference between this simulation and the literature value, it is conceivable to greatly increase the particle number and time scale. However, we think that it is difficult in terms of time cost to fill the difference efficiently in material design. Because IP2 is represented the simulation result that matches the molar volume of the literature value without considering the fast cooling rate of the simulation, it is considered that the distorted network structure is simulated. Although consistency between simulation results and literature values is very important, we believe that the material design simulation is required to the high reproducibility of tendency of structure and physical property corresponded with composition. The tendency of the molar volume corresponding the composition change of IP1 simulation improved the SiO_2 rich composition range

as compared with IP2 simulation. In addition, the composition dependences of the network structure (e.g. Q_n ratio) determined by the IP1 simulations are reasonable better than those of the IP2 simulations. Therefore, considering the particle number and the time scale difference of the actual system and simulation, we believe that the molar volumes of IP1. Comparing the thermal expansion calculated by IP1 and IP2 simulations with measured values, there is not much difference. This suggests that IP1 can simulate with the same precision as the determination method for fitting interatomic potential to literature values by trial and error like IP2.

The $\theta_{\text{Si-O-Si}}$ angle in silicate glasses has been reported to be distributed between 120° and 180° [12]; similarly, ^{17}O DAS-NMR investigation of $0.2K_2O$-$0.8SiO_2$ glass determined angles in the range of 120° or 130° to 180° [47]. The angle distributions determined in this work (Figure 5) are similar to the literature values [12, 47], and results of the IP1 simulations were more accurate than those of the IP2 simulations. Figure 8 shows the Si-O ring size distributions for the simulated $x$$Na_2O$-(1-$x$)$SiO_2$ glasses. The ring size is defined by the number of Si atoms in each ring. For the IP1 simulation with x = 0, six- to eight-membered rings were more abundant than small-sized rings, and the number of six- to eight-membered rings decreased with increasing x. In generally, three- to five-membered rings are considered to be composed of smaller angles than 6- to 8-membered rings. From Figures 6 and 8, it is considered highly likely that the three- to five-membered ring and the six- to eight-member ring correspond to the angle peaks of 140 ° and 160 °, respectively. Henderson et al. [13] reported that the nearest Si-Si distance became shorter with increasing x based on an investigation of the XANES Si-K-edge energy shifts in Na_2O-SiO_2 glasses; the observed shifts in $\theta_{\text{Si-O-Si}}$ angles in this work are consistent with these experimental results. In Figure 5, the distributions of

$\theta_{Si\text{-}O\text{-}Si}$ angles shift towards smaller angles with increasing x. On the other hand, there are more three-membered rings in glasses with x = 0.4 and 0.5 in the IP2 simulations compared to in the IP1 simulations; the presence of these three-membered rings in the IP2 simulations might reflect the distortion of the glass structure.

As shown in Figure 6, the Q_n ratios derived from the IP1 and IP2 simulations do not agree with the NMR result [46]. It is difficult to simulate using an enough cooling rate to reproduce the actual glass density in the MD simulation under *NPT* ensemble in the state close to real system. Moreover, there is a difference between the particle number of the model simulated and the calculation time compared with the real system. Therefore, it is conceivable that the calculated Q_n ratio value does not match the result of the actual system.

From the viewpoint of new glass material design, we think that it is important to reproduce the tendency of the structure and the physical properties corresponded with composition change from little or no experimental data. Since IP 1 is set using first principles calculation, we think that only basic crystal structure data can correspond to various compositions. IP1 is determined the interatomic potentials for each composition based on the results of the first-principles calculations and showed that the reproducibility of tendency of the structure and the physical property values of sodium silicate glasses with composition is better than IP2. We think that IP1 will be an effective determination method of interatomic potential for MD simulation of glass material design.

6. Summary

An interatomic potential for application in the classical MD simulation of sodium silicate glasses was developed using first-principles calculations. The ionic charges applied in the interatomic potential were determined by Mulliken population analyses of alkali silicate crystals. The Si-O interatomic potential was determined by fitting to a potential energy surface of an SiO^{2+} model established based on nonempirical MO calculations. The MD simulations using this new interatomic potential reproduced experimental trends in interatomic distance, molar volume, thermal expansion coefficient, Si-O-Si bond angle distribution, and Q_n ratio. Further investigation is needed to evaluate this improved interatomic potential for simulated glasses containing three or more components (e.g., sodium ions and other alkali ions).

References

[1] B.M. Wright, J.E. Shelby, Phase separation and the mixed alkali effect, Phys. Chem. Glasses 41 (2000) 192–198.

[2] R. Knoche, D.B. Dingwell, F.A. Seifert, S.L. Webb, Non-linear properties of supercooled liquids in the system Na_2O-SiO_2, Chem. Geol. 116 (1994) 1–16.

[3] J. Habasaki, I. Okada, Molecular dynamics study of Li_2SiO_3 in the liquid and glassy states, Mol. Sim. 8 (1992) 179–195.

[4] S. Tsuneyuki, M. Tsukada, H. Aoki, Y. Matsui, First-principles interatomic potential of silica applied to molecular dynamics, Phys. Rev. Lett. 61 (1988) 869–872.

[5] S. Tsuneyuki, Molecular dynamics simulation of silica with a first-principles interatomic potential, Mol. Engineer. 6

(1996) 157–182.

[6] G.J. Kramer, N.P. Farragher, B.W.H. van Besset, R.A. van Santen, Interatomic force fields for silicas, aluminophosphates, and zeolites:derivation based on *ab initio* calculations, Phys. Rev. B 43 (1991) 5068–5080.

[7] J. Habsaki, I. Okada, Molecular dynamics simulation of alkali silicates based on the quantum mechanical potential surfaces, Mol. Sim. 9 (1992) 319–326.

[8] S. Sakka, K. Matsusita, Studies on binary silicate glasses based on the SiKα and SiKβ emission X-rays, J. Non-Cryst. Solids 22 (1976) 57–66.

[9] F. Noritake, K. Kawamura, T. Yoshino, E. Takahashi, Molecular dynamics simulation and electrical conductivity measurement of $Na_2O \cdot 3SiO_2$ melt under high pressure; relationship between its structure and properties, J. Non-Cryst. Solids 358 (2012) 3109–3118.

[10] A.N. Cormack, J. Du, T.R. Zeitler, Sodium ion migration mechanisms in silicate glasses probed by molecular dynamics simulations, J. Non-Cryst. Solids 323 (2003) 147–154.

[11] N. Sawaguchi, K. Yamaguchi, M. Sasaki, K. Kawamura, Interatomic potential model for molecular dynamics simulation of lithium borate melts/glasses, J. Comput. Chem. Jpn. 14 (2015) 139–146.

[12] R.L. Mozzi, B.E. Warren, The structure of vitreous silica, J. Appl. Cryst. 2 (1969) 164–172.

[13] G.S. Henderson, A Si K-edge EXAFS/XANES study of sodium silicate glasses, J. Non-Cryst. Solids 183 (1995) 43–50.

[14] C. Mazzara, J. Jupille, A.-M. Flank, P. Lagarde, Stereochemical order around sodium in amorphous silica, J. Appl. Cryst. B 104 (2000) 3438–3445.

[15] G.N. Greaves, A. Fontaine, P. Lagarde, D. Raoux, S.J. Gurman, Local structure, of silicate glasses, Nature 293 (1981) 611–616.

[16] Y. Yamamoto, N. Sawaguchi, M. Sasaki, Interatomic potential for $x$$Na_2O$-(1–$x$)$SiO_2$ glasses, J. Comput. Chem., Jpn. 14 (2015) 63–66.

[17] H. Sakuma, K. Kawamura, Structure and dynamics of water on muscovite mica surfaces, Geochim. Cosmochim. Acta 73 (2009) 4100–4110.

[18] S.J. Clark, M.D. Segall, C.J. Pickard, P.J. Hasnip, M.J. Probert, K. Refson, M.C. Payne, First principles methods using CASTEP, Zeitschrift für Kristallographie, 220 (2005) 567–570.

[19] J.P. Perdew, K. Burke, M. Ernzerhof, Generalized gradient approximation made simple, Phys. Rev. Lett. **77** (1996) 3865–3868.

[20] A.F. Wright, M.S. Lehmann, The structure of quartz at 25 and 590 ℃ determined by neutron diffraction,J. Solid State Chem. 36 (1981) 371–380.

[21] H. Krüger, V. Kahlenberg, R. Kaindll, $Li_2Si_3O_7$: Crystal structure and Raman spectroscopy, J. Solid State Chem. 180 (2007) 922–928.

[22] B.H. de Jong, H.T. Supèr, A.L. Spek, N. Veldman, G. Nachtegaal, J.C. Fischer, Mixed alkali systems: Structure and ^{29}Si MASNMR of $Li_2Si_2O_5$ and $K_2Si_2O_5$, Acta Cryst. B54 (1998) 568–577.

[23] K.F. Hesse, Refinement of the crystal structure of lithium polysilicate, Acta Cryst. B33 (1977) 901–902.

[24] H. Voellenkle, A. Wittmann, H.N. Nowotny, Die kristallstruktur der verbindung $Li_6(Si_2O_7)$, Monatsh. Chem. 100 (1969) 295–303.

[25] R. Hoppe, K. Bernet, A. Moeller, Einkristall-Synthese hochschmelzender Oxyde bei niederer Temperatur: Gamma-($Li_4(SiO_4)$)-ohne Fehlordnung, isotyp mit $Na_4(SnO_4)$. (Was heisst 'Isotypie'?) Zeitschrift fuer Anorganische und Allgemenie Chemie, 629 (2003) 1285–1293.

[26] R. Hofmann, R. Hoppe, Ein neues Oxogermanat: $Li_8GeO_6 = Li_8O_2(GeO_4)$ (Mit einer Bemerkung ueber Li_8SiO_6 und Li_4GeO_4), Zeitschrift fuer Anorganische und Allgemeine Chemie, 555 (1987) 118–128.

[27] A.K. Pant, D.W.J. Cruickshank, The crystal structure of alpha-$Na_2Si_2O_5$, Acta Cryst. B24 (1968) 13–19.

[28] A. Grund, M.M. Pizy, Structure crystalline du metasilicate de sodium anhydre, Na_2SiO_3, Acta Cryst. 5 (1952) 837–840.

[29] W.H. Baur, E. Halwax, H. Voellenkle, Comparison of the crystal structures of sodium orthosilicate, Na_4SiO_4, and sodium orthogermanate Na_4GeO_4, Monatsh. Chem. 117 (1986) 793–797.

[30] M. Jansen, Zur kristallstruktur von kaliumdisilicat, Zeitschrift fuer Kristallographie, 160 (1982) 127–133.

[31] K. Bernet, R. Hoppe, Zur Kristallstruktur von K4(SiO4), Zeitschrift fuer Anorganische und Allgemeine Chemie 589 (1990) 129–138.

[32] E. Zintl, A. Harder, B. Dauth, Gitterstruktur der oxide, sulfide, selenide und telluride des lithiums, natriums und kaliums, Zeitschrift fuer Elektrochemie 40 (1934) 588–593.

[33] R.S. Mulliken, Electronic population analysis on LCAO-MO molecular wave functions. I, J. Chem. Phys. 23 (1955) 1833–1840.

[34] M.D. Segall, R. Shah, C.J. Pickard, M.C. Payne, Population analysis of plane-wave electronic structure calculations of bulk materials, Phys. Rev. B 54 (1996) 16317–16320.

[35] Y. Yamamoto, N. Sawaguchi, M. Sasaki, Interatomic potential for $x$$Li_2O$-(1-$x$)$SiO_2$ crystals, J. Comput. Chem., Jpn. 13 (2014) 173–174.

[36] F. L. Hirshfeld, Bonded-atom fragments for describing molecular charge densities, Theoret. Chim. Acta 44 (1977) 129–138.

[37] Gaussian 09, Revision **E.01**, M.J. Frisch, G.W. Trucks, H.B. Schlegel, G.E. Scuseria, M.A. Robb, J.R. Cheeseman, G. Scalmani, V. Barone, B. Mennucci, G.A. Petersson, H. Nakatsuji, M. Caricato, X. Li, H.P. Hratchian, A.F. Izmaylov, J. Bloino, G. Zheng, J.L. Sonnenberg, M. Hada, M. Ehara, K. Toyota, R. Fukuda, J. Hasegawa, M. Ishida, T. Nakajima, Y. Honda, O. Kitao, H. Nakai, T. Vreven, J. A. Montgomery, Jr., J.E. Peralta, F. Ogliaro, M. Bearpark, J.J. Heyd, E. Brothers, K.N. Kudin, V.N. Staroverov, R. Kobayashi, J. Normand, K. Raghavachari, A. Rendell, J.C. Burant, S.S. Iyengar, J. Tomasi, M. Cossi, N. Rega, J.M. Millam, M. Klene, J.E. Knox, J.B. Cross, V. Bakken, C. Adamo, J. Jaramillo, R. Gomperts, R.E. Stratmann, O. Yazyev, A.J. Austin, R. Cammi, C. Pomelli, J.W. Ochterski, R.L. Martin, K. Morokuma, V.G. Zakrzewski, G.A. Voth, P. Salvador, J.J. Dannenberg, S. Dapprich, A.D. Daniels, Ö. Farkas, J.B. Foresman, J.V. Ortiz, J. Cioslowski, D.J. Fox, Gaussian, Inc., Wallingford CT, 2009.

[38] M. Head-Gordon, J.A. Pople, M.J. Frisch, MP2 energy evaluation by direct methods, Chem. Phys. Lett. 153 (1988) 503–506.

[39] G.A. Petersson, A. Bennett, T.G. Tensfeldt, M.A. Al-Laham, W.A. Shirley, J. Mantzaris, A complete basis set model chemistry. I. The total energies of closed-shell atoms and hydrides of the first-row atoms, J. Chem. Phys. 89 (1988) 2193–2218.

[40] K. Kawamura, MXDORTO, Japan Chemistry Program Exchange P029, (1996).

[41] J. Du, A.N. Cormack, The medium range structure of sodium silicate glasses: A molecular dynamics simulation, J. Non-Cryst. Solids 349 (2004) 66–79.

[42] R.N. Mead, G. Mountjoy, A molecular dynamics study of the atomic structure of $(CaO)_x(SiO_2)_{1-x}$ glasses, J. Phys. Chem. B 110 (2006) 14273–14278.

[43] K. Takahashi, A. Osaka, Elastic properties of alkali silicate glasses, Yogyo-Kyokai-Shi, 91 (1983) 22–26.

[44] P.B. Narottam, R.H. Doremus, Handbool of glass properties, Acdemic Orlando, (1986).

[45] J.F. Stebbins, Identification of multiple structural species in silicate glasses by ^{29}Si NMR, Nature 330 (1987) 465–467.

[46] H. Maekawa, T. Maekawa, K. Kawamura, T. Yokokawa, The structural groups of alkali silicate glasses determined from ^{29}Si MAS-NMR, J. Non-Cryst. Solids 127 (1991) 53–64.

[47] I. Farnan, P.J. Grandinetti, J.H. Baltisberger, J.F. Stebbins, U. Werner, M.A. Eastman, A. Pines, Quantification of the disorder in network-modified silicate glasses, Nature 358 (1992) 31–35

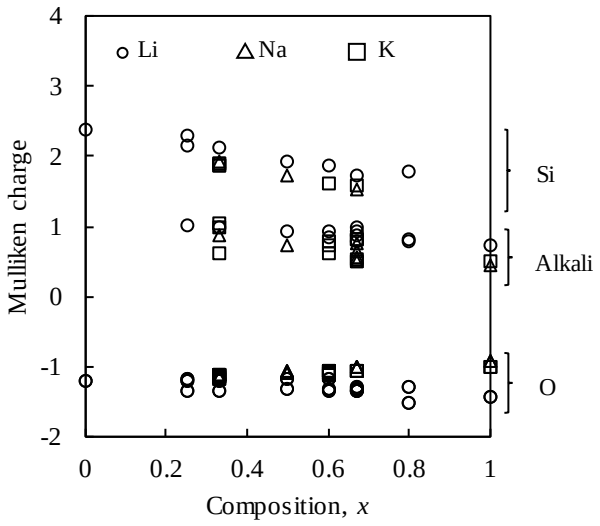

Figure 1: Mulliken charges of ions in several xA_2O-(1-x)SiO_2 crystals (listed in Table 1).

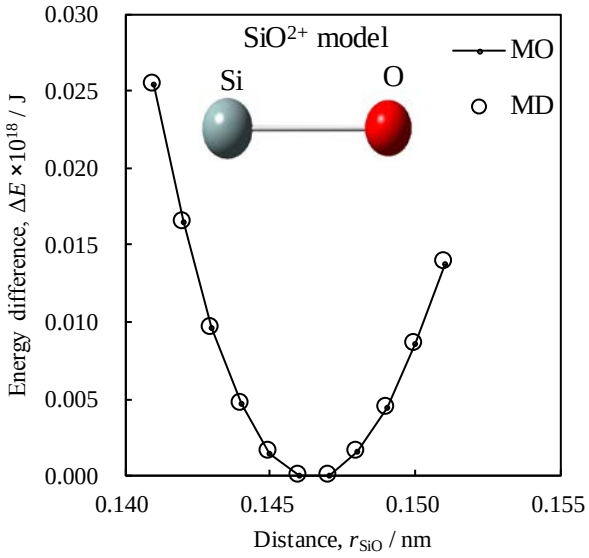

Figure 2: Energy surface determined from MO calculation (MP2/6-311+g(d)) of an SiO^{2+} model and potential energies calculated by (1) with fitted parameters for $x = 0$.

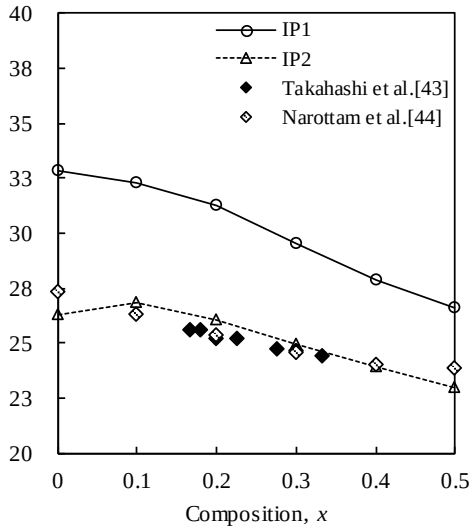

Figure 3: Molar volumes of $x$$Na_2O$-(1-$x$)$SiO_2$ glasses simulated at 300 K.

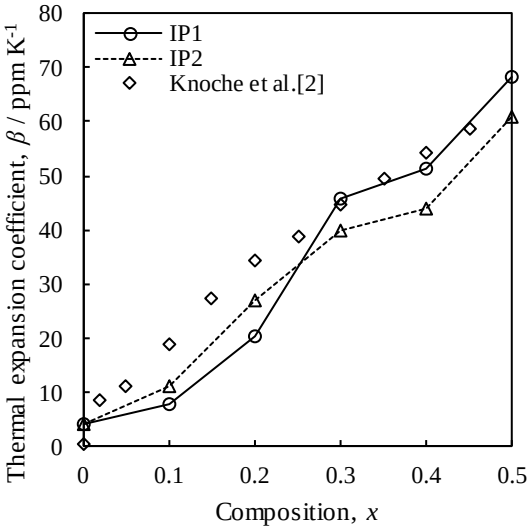

Figure 4: Thermal expansion coefficients of $x$$Na_2O$-(1-$x$)$SiO_2$ glasses obtained from simulations at 300 and 600 K.

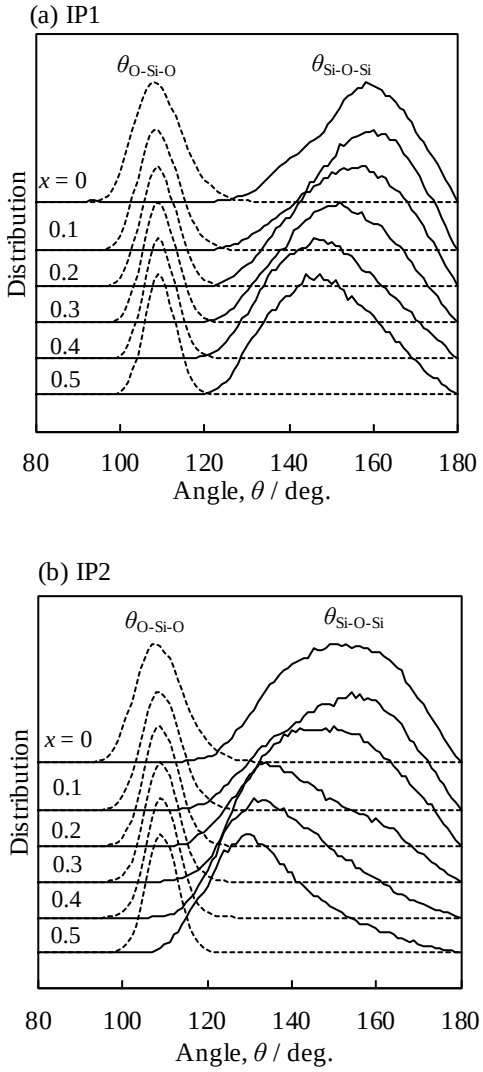

Figure 5: Distribution of O-Si-O ($\theta_{O\text{-}Si\text{-}O}$) and Si-O-Si ($\theta_{Si\text{-}O\text{-}Si}$) bond lengths in $x$$Na_2O$-(1-$x$)$SiO_2$ glasses simulated at 300 K using IP1 (a) and IP2 (b). Dashed and solid lines show $\theta_{O\text{-}Si\text{-}O}$ and $\theta_{Si\text{-}O\text{-}Si}$, respectively·

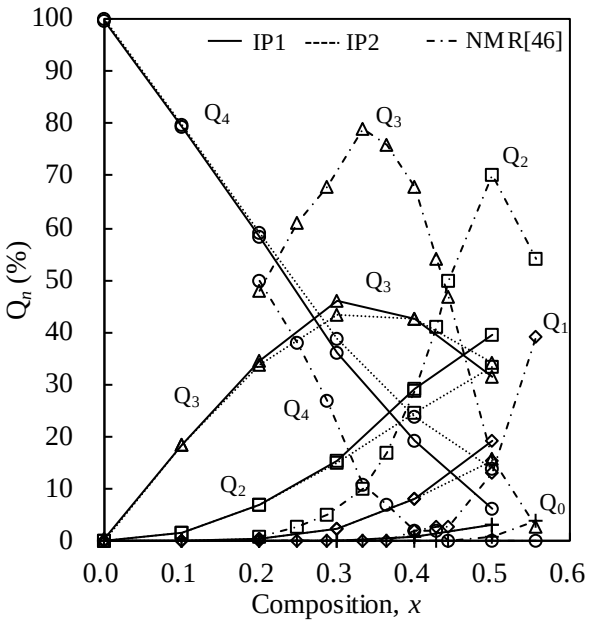

Figure 6: Q_n ratios in xNa$_2$O-(1-x)SiO$_2$ glasses simulated at 300 K (circles = Q_4, triangles = Q_3, squares = Q_2, diamonds = Q_1, and plus signs = Q_0).

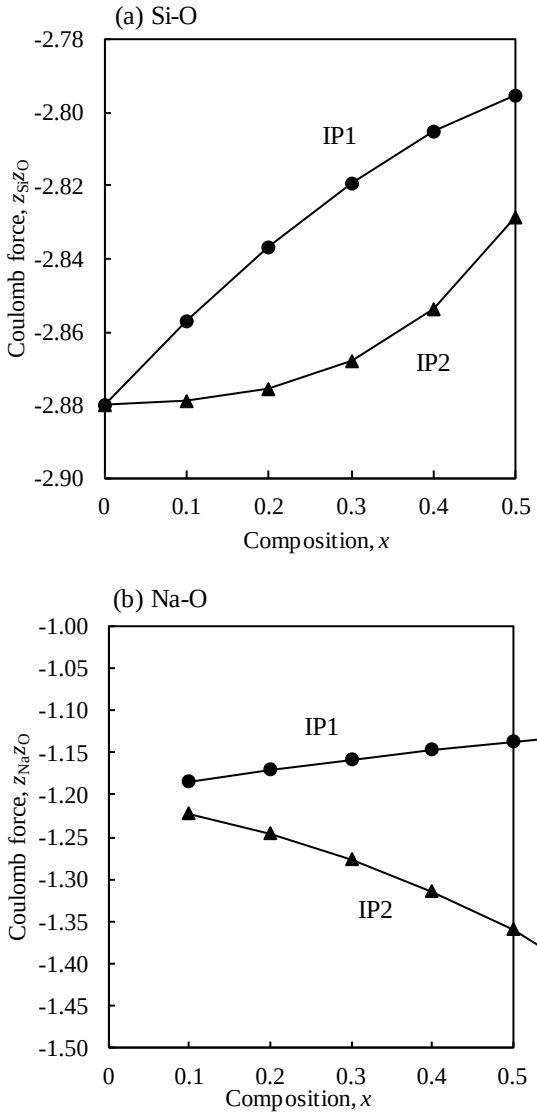

Figure 7: Si-O (a) and Na-O (b) of Coulomb force $z_i z_j$ (circles = IP1, triangles = IP2).

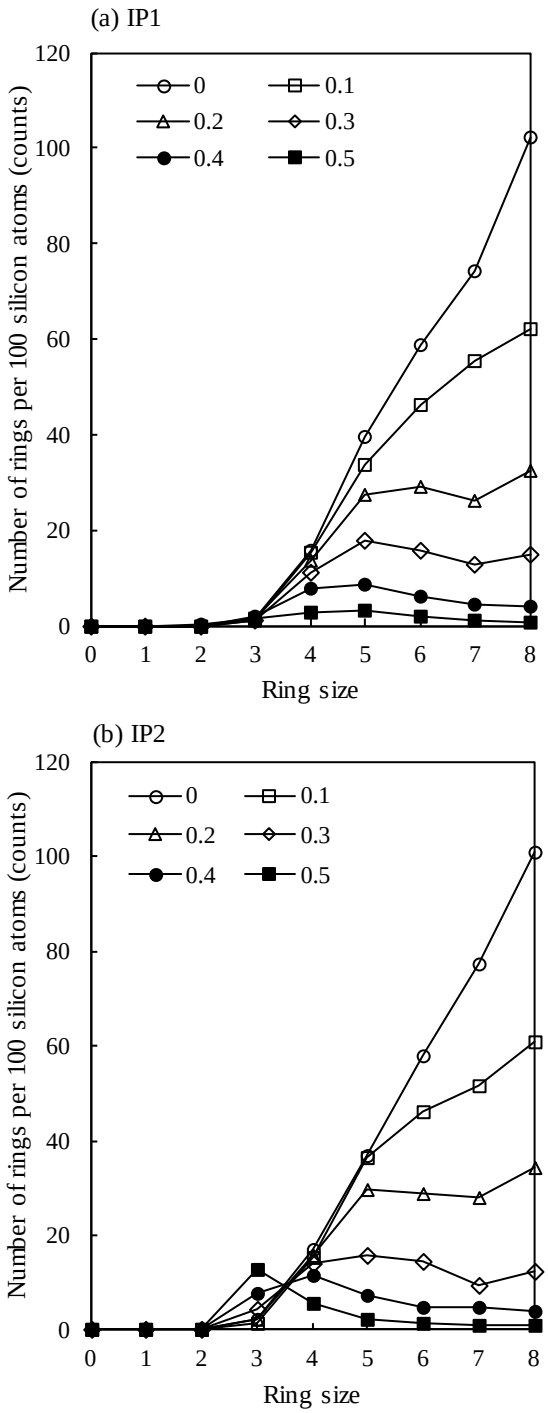

Figure 8: Ring size distributions in xNa$_2$O-(1-x)SiO$_2$ glasses simulated at 300 K using IP1 (a) and IP2 (b).

Tables

Table 1: The deviation denotes the difference of structural optimization by DFT.

Crystals	*ref.*	Lattice parameter (deviation, %)						*k*-points	Number of ions in cell
		a / nm	*b* / nm	*c* / nm	*α* / deg.	*β* / deg.	*γ* / deg.		
α-SiO_2	[20]	0.49134 (2.20)	0.49134 (2.20)	0.54052 (1.95)	90 (0)	90 (0)	120 (0)	3×3×4	9
$Li_2Si_3O_7$	[21]	1.9648 (1.27)	0.59969 (0.73)	0.48691 (1.37)	90 (0)	90 (0)	90 (0)	1×2×3	48
$Li_2Si_2O_5$	[22]	0.5807 (1.09)	1.4582 (1.30)	0.4773 (1.51)	90 (0)	90 (0)	90 (0)	2×1×3	36
Li_2SiO_3	[23]	0.9392 (0.47)	0.5397 (0.54)	0.466 (1.71)	90 (0)	90 (0)	90 (0)	2×3×3	24
$Li_6Si_2O_7$	[24]	0.7715 (0.67)	0.7715 (0.67)	0.488 (0.79)	90 (0)	90 (0)	90 (0)	2×2×3	30
Li_4SiO_4	[25]	0.7519 (0.74)	0.5648 (0.56)	0.5031 (0.61)	124.15 (0.05)	97.18 (0.21)	100.26 (0.34)	2×3×3	18
Li_8SiO_6	[26]	0.54243 (0.31)	0.54243 (0.31)	1.0626 (0.23)	90 (0)	90 (0)	120 (0)	3×3×2	30
$Na_2Si_2O_5$	[27]	0.6409 (1.35)	1.5422 (1.44)	0.4896 (1.40)	90 (0)	90 (0)	90 (0)	2×1×3	36
Na_2SiO_3	[28]	1.043 (2.11)	0.602 (2.63)	0.481 (1.50)	90 (0)	90 (0)	90 (0)	1×2×3	24
Na_4SiO_4	[29]	0.5576 (1.34)	0.5576 (1.47)	0.8393 (1.78)	80.92 (0.17)	71.84 (0.09)	67.44 (0.19)	3×3×2	18
$K_2Si_2O_5$	[22]	1.63224 (2.88)	1.1243 (1.25)	0.9919 (1.90)	90 (0)	115.97 (0.61)	90 (0)	1×1×2	108
$K_6Si_2O_7$	[30]	0.6458 (0.81)	0.8887 (0.75)	1.0879 (1.25)	90 (0)	125 (0.23)	90 (0)	3×2×2	30
K_4SiO_4	[31]	1.037 (0.74)	0.6392 (1.51)	1.0366 (0.88)	90 (0)	112.83 (0.63)	90 (0)	1×2×1	36
Li_2O	[32]	0.4628 (0.65)	0.4628 (0.65)	0.4628 (0.64)	90 (0)	90 (0)	90 (0)	4×4×4	12
Na_2O	[32]	0.555 (1.24)	0.555 (1.24)	0.555 (1.24)	90 (0)	90 (0)	90 (0)	4×4×4	12
K_2O	[32]	0.6436 (0.74)	0.6436 (0.74)	0.6436 (0.74)	90 (0)	90 (0)	90 (0)	2×2×2	12

Table 2: Determined interatomic potential parameters for the simulation of $x$$Na_2O$-(1-$x$)$SiO_2$ glasses.

(a) IP1

x = 0	z	a / nm	b / nm	c / (kJ mol)$^{1/2}$ nm^3
O	neutrality	0.18464	0.01411	0.05605
Si	–0.50x+2.4	0.10007	0.00799	0.00000
	D_{1ij} / kJ mol^{-1}	β_{1ij} / nm^{-1}	D_{2ij} / kJ mol^{-1}	β_{2ij} / nm^{-1}
Si-O	627600.00	52.05	83680.00	34.21

x = 0.1	z	a / nm	b / nm	c / (kJ mol)$^{1/2}$ nm^3
O	neutrality	0.18421	0.01401	0.05605
Si	–0.50x+2.4	0.09967	0.00798	0.00000
	D_{1ij} / kJ mol^{-1}	β_{1ij} / nm^{-1}	D_{2ij} / kJ mol^{-1}	β_{2ij} / nm^{-1}
Si-O	627600.00	52.06	83680.00	34.20

x = 0.2	z	a / nm	b / nm	c / (kJ mol)$^{1/2}$ nm^3
O	neutrality	0.18397	0.01396	0.05605
Si	–0.50x+2.4	0.09944	0.00797	0.00000
	D_{1ij} / kJ mol^{-1}	β_{1ij} / nm^{-1}	D_{2ij} / kJ mol^{-1}	β_{2ij} / nm^{-1}
Si-O	627600.00	52.06	83680.00	34.19

x = 0.3	z	a / nm	b / nm	c / (kJ mol)$^{1/2}$ nm^3
O	neutrality	0.18362	0.01391	0.05605
Si	–0.50x+2.4	0.09930	0.00797	0.00000
	D_{1ij} / kJ mol^{-1}	β_{1ij} / nm^{-1}	D_{2ij} / kJ mol^{-1}	β_{2ij} / nm^{-1}
Si-O	627650.21	52.01	83680.00	34.17

x = 0.4	z	a / nm	b / nm	c / (kJ mol)$^{1/2}$ nm^3
O	neutrality	0.18326	0.01386	0.05605
Si	$-0.50x+2.4$	0.09914	0.00796	0.00000
	D_{1ij} / kJ mol^{-1}	β_{1ij} / nm^{-1}	D_{2ij} / kJ mol^{-1}	β_{2ij} / nm^{-1}
Si-O	627696.23	51.96	83680.00	34.15

x = 0.5	z	a / nm	b / nm	c / (kJ mol)$^{1/2}$ nm^3
O	neutrality	0.18300	0.01383	0.05605
Si	$-0.50x+2.4$	0.09902	0.00796	0.00000
	D_{1ij} / kJ mol^{-1}	β_{1ij} / nm^{-1}	D_{2ij} / kJ mol^{-1}	β_{2ij} / nm^{-1}
Si-O	627725.52	51.92	83680.00	34.14

	z	a / nm	b / nm	c / (kJ mol)$^{1/2}$ nm^3
Na	$-0.25x+1.0$	0.13220	0.01150	0.01227

(b) IP2

	z[11]	a / nm	b / nm	c / (kJ mol)$^{1/2}$ nm^3
O	neutrality	0.18610	0.01510	0.05605
Si	$2.4+1.6x/(3x-4)$	0.10120	0.00830	0.00000
Na	1.0000	0.13220	0.01150	0.01227
	D_{1ij} / kJ mol^{-1}	β_{1ij} / nm^{-1}	D_{2ij} / kJ mol^{-1}	β_{2ij} / nm^{-1}
Si-O	222170.40	50.00	13849.04	22.40

Table 3: Si-O and Na-O bond lengths in $x$$Na_2O$-(1-$x$)$SiO_2$ glasses estimated from the pair correlation function simulated at 300 K.

x		Distance / nm		
		IP1	IP2	References
0	d_{Si-O}	0.164	0.157	0.162(g)[a] / 0.1608(g)[b] / 0.159(c)[c]
0.1	d_{Si-O}	0.164	0.157	———
	d_{Na-O}	0.225	0.221	0.232(g)[d]
0.2	d_{Si-O}	0.164	0.157	0.1617(g)[b]
	d_{Na-O}	0.226	0.225	———
0.3	d_{Si-O}	0.164	0.157	0.1668(g)[b] / 0.163(g)[e†] / 0.156-0.163(c)[f†]
	d_{Na-O}	0.230	0.227	0.235(g)[e†] / 0.228-0.237(c)[f†]
0.4	d_{Si-O}	0.164	0.158	0.1586(g)[b]
	d_{Na-O}	0.231	0.225	———
0.5	d_{Si-O}	0.164	0.158	0.155-0.167(c)[g]
	d_{Na-O}	0.232	0.223	0.224-0.244(c)[g]

(g) : glass (c) : crystal † x = 0.33

[a] *ref.* [12] [b] *ref.* [13] [c] *ref.* [20] [d] *ref.* [14] [e] *ref.* [15] [f] *ref.* [27] [g] *ref.* [28]